JOURNAL OF AIRCRAFT
Vol. 42, No. 6, November–December 2005

Optimum Two-Per-Revolution Inputs for Improved Rotor Performance

Rendy P. Cheng* and Roberto Celi†
University of Maryland, College Park, Maryland 20742

The results of a study to determine the optimum two-per-revolution blade control inputs required to minimize rotor power, maximize thrust, or minimize rotor speed, using formal numerical optimization techniques, are presented. The impact of improved rotor modeling on the prediction of the effects of two-per-revolution input on rotor power is also addressed, in particular, the effect of using a free wake inflow model, and a flexible rotor blade model. The main conclusions of the present study are as follows: The optimization for optimum two-per-revolution input is best carried out by solving the trim problem for every value of the inputs proposed by the optimizer, as opposed to integrating the trim calculations as equality constraints in the optimization. An appropriate two-per-revolution input can increase the rotor maximum thrust at high speed by about 11%. The additional thrust is generated at the front and the rear of the rotor disk. The two-per-revolution input can also further reduce the rotor speed compared with a case without such input. The physical mechanism is the same as in the optimization for maximum thrust, and the maximum value of C_T/σ is also the same. Although the power predictions obtained using a free wake model are different from those obtained with a simpler linear inflow model, the accuracy of the optimum two-per-revolution input predicted using the simpler model is adequate. The best practical strategy to optimize the two-per-revolution input is to conduct an initial study with a simple linear inflow model and then refine it with the more sophisticated one. The same conclusions hold for more sophisticated flexible blade models, compared with simpler rigid blade ones.

Nomenclature

A_2	=	amplitude of the two-per-revolution input, deg
C_D	=	airfoil profile drag coefficient
C_L	=	airfoil local lift coefficient
C_T	=	thrust coefficient
DV	=	design variable
M	=	Mach number
P_{MR}	=	main rotor required power
r	=	blade radial station, ft
α	=	angle of attack, deg
μ	=	advance ratio
σ	=	rotor solidity
ϕ_2	=	phase of two-per-revolution input, deg
ψ	=	blade azimuth angle, deg
Ω	=	rotor speed, rad/s

Introduction

HIGHER harmonic control (HHC) of helicopter rotor blades has received increasing attention over the last two decades, especially as a means of alleviating vibratory loads and reducing noise. Various actuating schemes have been proposed, including high-frequency actuators in the fuselage, active pitch links, trailing-edge flaps, spoilers, and leading-edge elevons. Typically the input frequency has been N/per revolution, where N is the number of rotor blades, but other frequencies have also been utilized. A detailed survey of the extensive work in the area is beyond the scope of this paper; recent comprehensive reviews have been presented by Friedmann and Millot[1] and Teves et al.[2]

In most of these studies, the primary objective of HHC was vibration or noise reduction. The effects of HHC on rotor performance measures such as rotor thrust and required power were studied primarily to ensure that the optimum HHC input would not degrade the overall performance of the rotor. Only a few studies have specifically focused on the use of HHC for rotor performance improvement.

Pioneering analytical studies in the 1950s and early 1960s by Stewart,[3] Payne,[4] and Arcidiacono[5] showed the potential effectiveness of HHC in alleviating retreating blade stall. Interest in the topic waned for about two decades. Starting from the late 1970s, extensive research on the use of HHC implemented in the form of individual blade control (IBC) was carried out by Ham and is summarized in Ref. 6. One of the many potential applications of IBC proposed was stall alleviation and performance enhancement,[7] which was accomplished through the superposition of two- and three-per-revolution pitch inputs applied in the rotating system.

Shaw et al.[8] describe wind-tunnel tests on a scaled three-bladed CH-47D rotor that addressed the effects of HHC on both vibration and performance. The results indicated a 6% reduction in power at 135 kn and a 4% reduction in power at 160 kn with a properly phased two-per-revolution input. A theoretical study of a similar configuration was carried out by Nguyen and Chopra.[9] The study confirmed that a properly phased two-per-revolution input can reduce rotor power, but at the expense of increased vibratory hub shears. Polychroniadis[10] discusses the application of HHC to an Aerospatiale SA-349 Gazelle for vibration and noise reduction and includes a performance analysis based on both theoretical studies and wind-tunnel testing. The theoretical results indicate a 22% increase in rotor thrust at an advance ratio $\mu = 0.5$, primarily caused by the alleviation of retreating blade stall, but much smaller gains at lower values of μ. Wind-tunnel tests on a model rotor show that a power reduction of about 5% is possible with a two-per-revolution input. Jacklin et al.[11,12] describe full-scale BO-105 wind-tunnel tests to evaluate the effects of IBC at various frequencies on rotor performance, vibrations, and acoustics. With a two-per-revolution input, up to 7% power reductions were observed at high advance ratios, but none were seen for lower cruise speeds.

Cheng et al.[13] have studied the effects of a two-per-revolution input on rotor power and explored some of the underlying physical mechanisms. The results have shown that a properly phased two-per-revolution input can reduce the rotor required power by up to

Received 17 August 2002; revision received 3 September 2003; accepted for publication 8 September 2003.

*Graduate Research Assistant, Department of Aerospace Engineering, Alfred Gessow Rotorcraft Center.

†Professor, Department of Aerospace Engineering, Alfred Gessow Rotorcraft Center.

11%. The improvements become significant only at high speed and weight. The primary physical mechanism is the change in distribution of the profile drag coefficient C_D over the rotor disk. The effect of the two-per-revolution input on thrust was not addressed, and the simulation model was limited to linear inflow and rigid rotor blades.

The present paper has two main objectives:

1) The optimum two-per-revolution input required to minimize rotor power, maximize thrust, or minimize rotor speed will be determined. This will be accomplished through formal numerical optimization techniques, rather than through parametric studies as in the rotor power calculations of Ref. 13.

2) The impact of improved rotor modeling on the prediction of the effects of two-per-revolution input on rotor power will be assessed. This will be accomplished by repeating some of the parametric studies of Ref. 13 with a free wake inflow model and with a flexible rotor blade model.

Mathematical Model of the Helicopter

The mathematical model of the helicopter used in this study is based on a set of coupled nonlinear rotor–fuselage equations in first-order, state-space form. The rigid-body dynamics of the helicopter are modeled with nonlinear Euler equations. The rotor model describes the dynamics of each blade with rigid-body coupled flap and lag degrees of freedom. Main rotor inflow is calculated using a three-state dynamic inflow model that yields linear inflow distribution over the rotor disk. Tip losses are taken into account under the assumption that the outboard 3% of the blade does not generate aerodynamic loads. A one-state dynamic inflow model is used for the tail rotor. All of the results presented in the paper were obtained from a coupled rotor–fuselage trim procedure simulating free-flight conditions. The trim procedure enforces force and moment equilibrium about the body axes and periodicity of the rotor blade motion. The trim unknowns are the main rotor and tail rotor pitch settings, roll and pitch angle, angle of attack and sideslip, and the harmonics of the flap and lag blade motion. Additional details of the mathematical model, including validation results, can be found in Refs. 14 and 15.

The geometric pitch angle θ_G of the blade is given by

$$\theta_G(\psi) = \theta_0 + \theta_{1c}\cos(\psi + \Delta_{\text{sp}}) + \theta_{1s}\sin(\psi + \Delta_{\text{sp}}) + \theta_2(\psi) \quad (1)$$

where θ_0, θ_{1c}, and θ_{1s} are, respectively, the collective, lateral cyclic, and longitudinal cyclic pitch; Δ_{sp} is the swashplate phasing angle ($\Delta_{\text{sp}} = -9.7$ deg in present study); and $\theta_2(\psi)$ is the two-per-revolution input, defined as

$$\theta_2(\psi) = A_2\cos(2\psi - \phi_2 + \Delta_{\text{sp}}) \quad (2)$$

Formulation of the Performance Optimization Problems

A primary objective of the present study was to determine the optimum magnitude and phase of the two-per-revolution input for three cases, namely, minimum rotor power, maximum thrust, and minimum rotor speed. In all three cases, the helicopter must remain in trim as the optimization algorithm selects the optimum values of the input.

Optimization for Minimum Power

In the first attempt to formulate the optimization problem, the trim equations were included directly in the form of equality constraints $h(\boldsymbol{X})$. (Recall that the trim problem is formulated as a set of nonlinear algebraic equations.) The trim unknowns $\boldsymbol{X}$ were included as design variables. Therefore, the optimization problem was formulated as follows: Minimize the main rotor power P_{MR}

$$F(\boldsymbol{X}) = P_{\text{MR}} \rightarrow \min$$

Subject to

$$h_j(\boldsymbol{X}) = 0, \qquad j = 1, \ldots, 29$$

Of the 29 equality constraints, 11 represented the trim conditions for the entire aircraft, 4 for the inflow trim equations, and 14 for the main rotor equations. The vector $\boldsymbol{X}$ of design variables was composed of 31 elements, namely, the 29 trim variables and the sine and cosine magnitudes of the two-per-revolution input as listed in Table 1. The initial solution was obtained from an algebraic trim procedure without a two-per-revolution input, and therefore, it was always feasible. The optimization was carried out with a modified method of feasible directions,[16] as implemented in the code DOT.[17] The numerical properties of this formulation proved to be extremely poor. Convergence was very slow, and the software often terminated the optimization for lack of progress. After unsuccessfully trying several variations of the baseline process, this formulation was abandoned.

Table 1 Design variables for the optimization procedure

Parameter	Symbol
Lateral cyclic	δ_{lat}
Longitudinal cyclic	δ_{lon}
Collective	δ_{col}
Tail rotor collective	δ_{ped}
Aerodynamic angle of attack	α_F
Fuselage sideslip angle	β_F
Fuselage roll attitude	ϕ_F
Fuselage pitch attitude	θ_F
Uniform component of main rotor inflow	λ_0
Cosine component of main rotor inflow	λ_c
Sine component of main rotor inflow	λ_s
Uniform component of tail rotor inflow	λ_t
Fuselage downwash	v_x
Fuselage sidewash	v_y
Engine torque	τ_{eng}
Constant portion of blade flapping mode	β_0
First harmonic cos of blade flapping mode	β_{1c}
First harmonic sin of blade flapping mode	β_{1s}
Second harmonic cos of blade flapping mode	β_{2c}
Second harmonic sin of blade flapping mode	β_{2s}
Third harmonic cos of blade flapping mode	β_{3c}
Third harmonic sin of blade flapping mode	β_{3s}
Constant portion of blade lead-lag mode	ζ_0
First harmonic cos of blade lead-lag mode	ζ_{1c}
First harmonic sin of blade lead-lag mode	ζ_{1s}
Second harmonic cos of blade lead-lag mode	ζ_{2c}
Second harmonic sin of blade lead-lag mode	ζ_{2s}
Third harmonic cos of blade lead-lag mode	ζ_{3c}
Third harmonic sin of blade lead-lag mode	ζ_{3s}
Cos magnitudes of the two-per-revolution input	A_{2c}
Sin magnitudes of the two-per-revolution input	A_{2s}

A different approach to the optimization process proved much more successful. For the minimum power optimization, the problem was formulated as an unconstrained minimization:

$$F(\boldsymbol{X}) = P_{\text{MR}} \rightarrow \min$$

with a vector $\boldsymbol{X}$ of design variables consisting of just two elements, namely, the sine and cosine magnitudes of the two-per-revolution input. This way, the trim procedure was decoupled from the optimization, and it was simply executed separately for every value of $\boldsymbol{X}$ proposed by the optimizer. The optimization was carried out using a Broyden–Fletcher–Goldfarb–Shanno algorithm (see Ref. 16) as implemented in the code DOT.[17]

Optimization for Maximum Thrust

The effects of the two-per-revolution input on rotor thrust cannot be assessed as directly as those on power when using a free-flight trim simulation. In fact, rotor thrust is an output of the trim procedure. Regardless of the presence or absence of the two-per-revolution input, the trim procedure will always make the rotor generate the amount of thrust required to achieve the appropriate force and moment equilibrium. To evaluate the effects of two-per-revolution input on the maximum rotor thrust capabilities at a given flight speed, it was necessary to repeat the trim procedure with increasing values of the weight of the helicopter.

The maximum thrust optimization was carried out by increasing the helicopter weight in 100-lb increments, starting from 22,000 lb

until the helicopter could no longer be trimmed. For each value of the weight, the two-per-revolution input for minimum power was calculated as indicated in the preceding section.

Optimization for Minimum Rotor Speed

The minimum rotor speed optimization was carried out by decreasing the rotor speed in steps of 0.2 rad/s from the nominal value of 27 rad/s, until the helicopter could no longer be trimmed. The procedure was repeated for increasing values of the weight, until the rotor speed could no longer be reduced below its nominal value. For each value of the rotor speed, the two-per-revolution input for minimum rotor power was calculated as described earlier. Rotor speed can obviously be decreased even without a two-per-revolution input. Therefore, for comparison purposes, the minimum rotor speed without the two-per-revolution input was also calculated for each value of the weight, again by decreasing the rotor speed in steps of 0.2 rad/s from the nominal value, until the helicopter could no longer be trimmed.

Optimization Results

This section presents results obtained for a helicopter similar to the Sikorsky UH-60 Blackhawk, except that the blade is assumed to be straight, that is, with zero tip sweep. The blade dynamics consist of rigid blade flap and lag motions only, torsion and flexible flap and lag modes have not been included. Stall and compressibility effects are incorporated in a quasi-steady form, and unsteady aerodynamic effects have been neglected. Linear inflow is assumed over the disk. All of the preceding simplifying assumptions should be taken into account in evaluating the results of the present study: Blade flexibility, unsteady aerodynamics, and nonlinear inflow all affect, to some extent, the lift and drag distributions over the rotor disk and, therefore, the power and thrust characteristics of the rotor. Unless noted otherwise, the rotor speed is constant, and there is no limitation on the power supplied by the engine.

Optimum Input for Minimum Power

Two slightly different optimizations were performed for the minimum rotor power case. In the first, only one design variable was used, namely, the phase ϕ_2 of the two-per-revolution input. The amplitude A_2 was held fixed to 1 deg. The optimum two-per-revolution phase angle for 16,000 and 22,000 lb were found to be 212 deg and 80 deg, respectively. These optimum solutions are shown in Figs. 1 and 2, together with the results of the parametric study: The open circles represent the results of the parametric study, and the solid circles represent the optimum solution.

In the second optimization, both A_2 and ϕ_2 were used. More precisely, the design variables were the cosine and sine components θ_{2c} and θ_{2s}, where $\theta_{2c} = A_2 \cos\phi_2$ and $\theta_{2s} = A_2 \sin\phi_2$. The optimum two-per-revolution inputs for 16,000 and 22,000 lb are $A_2 = 1.2$ deg and $\phi_2 = 210$ deg and $A_2 = 1.1$ deg and $\phi_2 = 86$ deg, respectively.

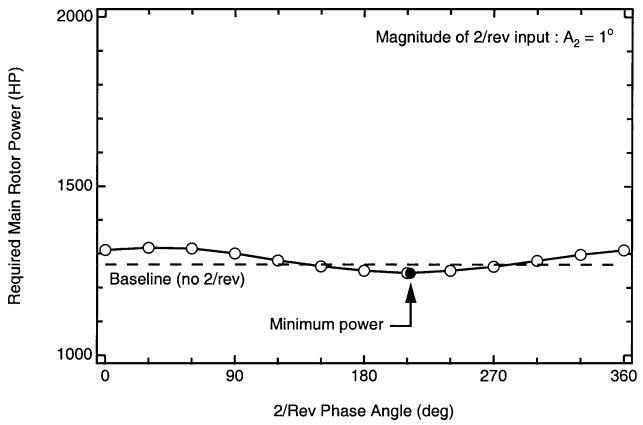

Fig. 1 Optimum two-per-revolution phase angle for minimum power, 16,000 lb and 120 kn.

Table 2 Optimum two-per-revolution input for minimum power

Design variable (DV)	Parametric study	DV 1	DV 2
		16,000-lb case	
Two-per-revolution amplitude	1 deg	1 deg	1.24 deg
Two-per-revolution phase	210.0 deg	212.22 deg	210.14 deg
Power reduction	1.97%	1.98%	2.07%
		22,000-lb case	
Two-per-revolution amplitude	1 deg	1 deg	1.05 deg
Two-per-revolution phase	90.0 deg	80.47 deg	86.23 deg
Power reduction	11.2%	11.3%	11.3%

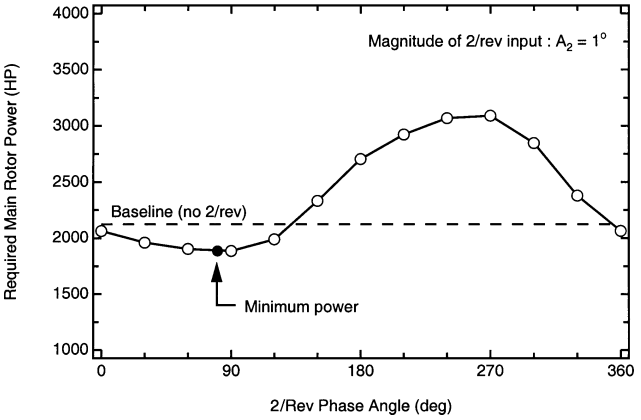

Fig. 2 Optimum two-per-revolution phase angle for minimum power, 22,000 lb and 120 kn.

The results of the one- and two-design variable cases are summarized in Table 2.

The values obtained with formal optimization techniques are very close to the best obtained from the parametric study, which indicates that the optimization is performed correctly. Because the two types of results are so close, the underlying physical mechanisms are the same as described in Ref. 13 and will not be further discussed here.

Optimum Input for Maximum Rotor Thrust

With the optimum values of the two-per-revolution input of $A_2 = 2.4$ deg and $\phi_2 = 56$ deg, it was possible to obtain a maximum trimmable weight of 24,500 lb at the desired speed of 120 kn. These values correspond to an advance ratio $\mu = 0.28$ and a thrust coefficient $C_T/\sigma = 0.115$. At the same speed, the simulation used in the present study generated a trim solution up to a maximum weight of 22,000 lb without two-per-revolution input.[13] Therefore, the two-per-revolution input allows a weight increase of 2500 lb, or 11.4% of the baseline value.

The reason for this increase can be identified by looking at the angle-of-attack distribution over the rotor disk, shown in Fig. 3. (In all rotor maps, the position $\psi = 0$ deg, corresponding to the tail of the helicopter, is at the bottom of the disk.) Figure 3a shows the distribution for the maximum trimmable weight case with the optimum two-per-revolution input. Figure 3b is the maximum trimmable weight case without the two-per-revolution input (baseline case). Figure 3c is the difference between these two cases. Looking at the angle-of-attack distribution of the baseline case, it is clear that the rotor is operating with large stall regions, especially on the retreating side. The stall, therefore, limits the maximum weight. As shown in Fig. 3c, the optimum two-per-revolution input increases the angle of attack in the second and fourth quadrant and decreases it in the first and third quadrants.

The changes in distribution of angle of attack have repercussions on the lift distribution. Figure 4 shows rotor maps of the $C_l M^2$ distribution. C_l is the local lift coefficient, and $C_l M^2$ is proportional to the local lift. The Fig. 4a rotor map refers to the maximum rotor thrust case, Fig. 4b refers to the baseline case, and Fig. 4c is the difference $\Delta C_l M^2$ between the two. Figure 4c indicates that the optimum two-per-revolution input makes the front and rear parts of the disk lift

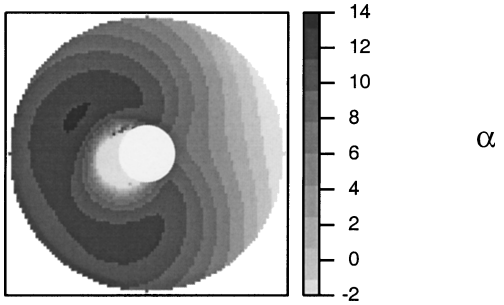

a) 24,500 lb; $A_2 = 2.42$ deg; and $\phi_2 = 55.48$ deg

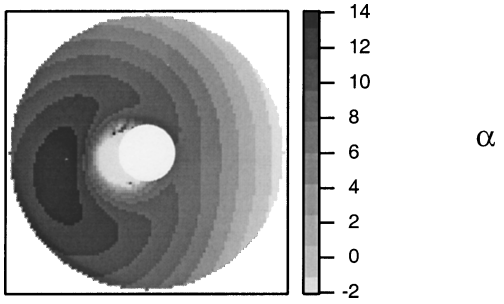

b) 22,000 lb and no two-per-revolution input

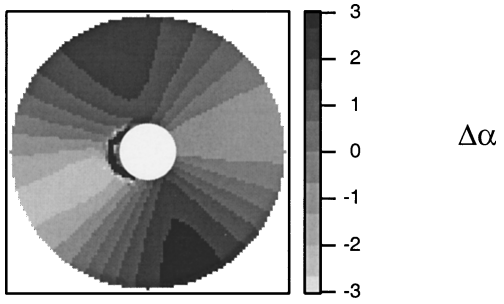

c) Difference in angle of attack

Fig. 3 Effect of optimum two-per-revolution input on angle-of-attack distribution, 120 kn.

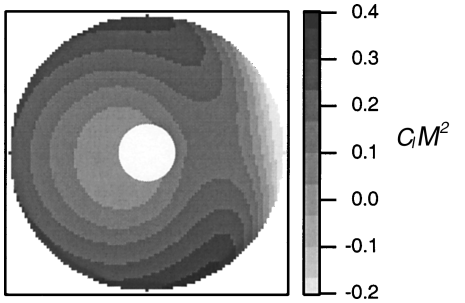

a) 24,500 lb; $A_2 = 2.42$ deg; and $\phi_2 = 55.48$ deg

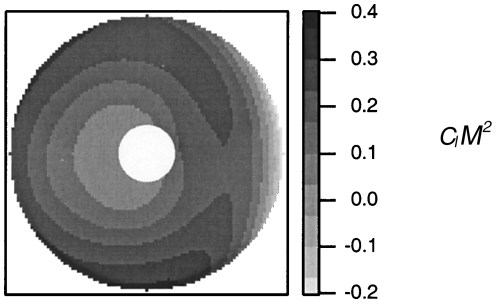

b) 22,000 lb and no two-per-revolution input

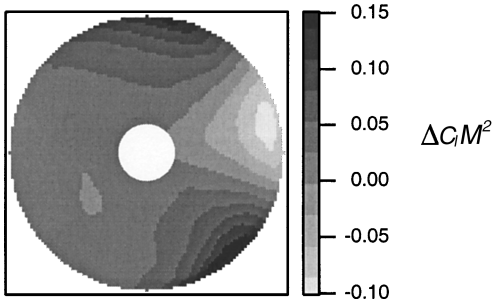

c) Difference in local lift

Fig. 4 Local lift distribution, 120 kn.

more, whereas it downloads the retreating and, especially, the advancing side. Overall, the region in which C_lM^2 increases is broader than where it decreases; therefore, the lift capability improves.

Note that the optimization was carried out under the assumption of unlimited available power. Achieving this maximum rotor thrust requires 3232 hp, which is of the order of the maximum takeoff power of the Sikorsky UH-60. Therefore, the power requirement is not unrealistically high.

Optimum Input for Minimum Rotor Speed

Figure 5 summarizes the results of the optimization study for minimum rotor speed. Note that the rotor speed was not varied continuously, but rather in discrete decrements of 0.2 rad/s from the nominal rotor speed of 27 rad/s. The open symbols refer to the baseline case; the solid symbols refer to the case with the two-per-revolution input applied. Four pairs of curves appear in Fig. 5, for weights of 16,000; 18,000; 20,000; and 22,000 lb. Figure 5 clearly shows that a two-per-revolution input allows a reduction of the rotor speed compared with the baseline case. Reducing rotor speed for a given helicopter weight, and, therefore, at essentially constant thrust, is equivalent to increasing the rotor loading C_T/σ, and it has just been shown that an appropriate two-per-revolution input increases the maximum achievable C_T/σ. Therefore, it is not surprising that an appropriate two-per-revolution input can reduce the minimum achievable rotor speed. From the results of Fig. 5, it appears that further reductions are not possible because of the thrust limits of the rotor, rather than a lack of available power.

Consider, for example, the 22,000-lb case: Without the two-per-revolution input, it is only possible to reduce the rotor speed by

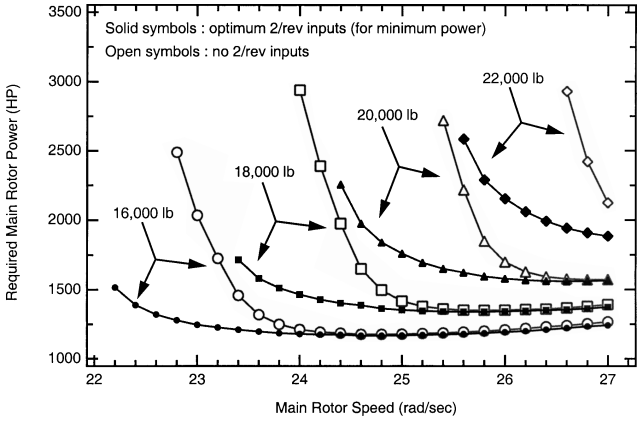

Fig. 5 Effect of two-per-revolution input on rotor power and minimum rotor speed for various helicopter weights, 120 kn.

0.4 rad/s below the nominal value of 27 rad/s. However, with a two-per-revolution input, the rotor speed can be reduced by 1.4 rad/s to 25.6 rad/s. The optimum two-per-revolution input for this minimum rotor speed is $A_2 = 2.3$ deg and $\phi_2 = 57$ deg. The required power increases rapidly as rotor speed is reduced, most likely because larger stall regions appear on the rotor disk. A similar trend can also be observed for all of the other values of the weight. Compare two cases with optimum two-per-revolution inputs, namely, 1) minimum rotor speed at the nominal weight and 2) nominal rotor speed at the maximum weight.

The nominal rotor speed is $\Omega = 27$ rad/s, and the nominal weight is 22,000 lb. The aircraft speed is 120 kn, corresponding to $\mu = 0.28$. The blade loading, C_T/σ, is essentially the same in both cases, but it is achieved by minimizing rotor speed in case 1 and maximizing thrust in case 2. Figure 6 shows angle-of-attack distribution over the rotor disk. The top rotor map shows the distribution for the minimum rotor speed case, and the bottom map is for the maximum rotor thrust case. The angle-of-attack distributions are similar, although not identical.

Similar results can also be seen in C_d, $C_d M^2$, and $r C_d M^2 \cos\phi\,\Omega$ distribution in Figs. 7–9. The term $r C_d M^2 \cos\phi\Omega$ represents the local profile power distribution, where ϕ is the local induced angle of attack. Because each case has a different rotor speed, $r C_d M^2 \cos\phi$ was premultiplied with individual Ω before the comparison.

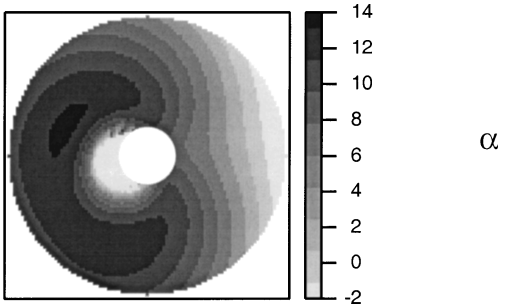

a) 22,000 lb; $\Omega = 25.6$ rad/s; $A_2 = 2.34$ deg; and $\phi_2 = 56.65$ deg

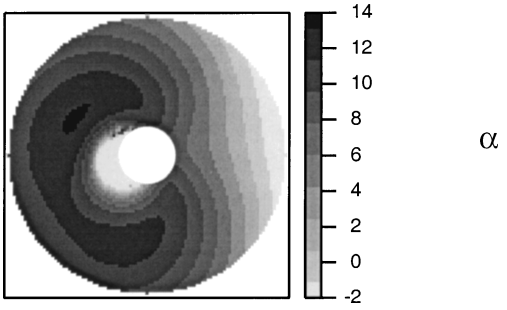

b) 24,500 lb; $\Omega = 27$ rad/s; $A_2 = 2.42$ deg; and $\phi_2 = 55.48$ deg

Fig. 6 Angle-of-attack distribution at maximum C_T/σ, 120 kn.

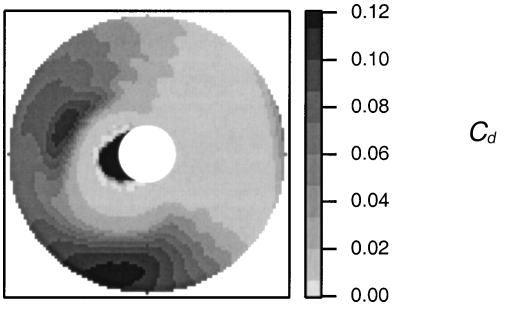

a) 22,000 lb; $\Omega = 25.6$ rad/s; $A_2 = 2.34$ deg; and $\phi_2 = 56.65$ deg

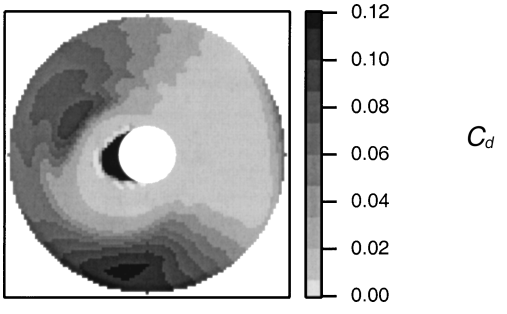

b) 24,500 lb; $\Omega = 27$ rad/s; $A_2 = 2.42$ deg; and $\phi_2 = 55.48$ deg

Fig. 7 Local drag coefficient distribution at maximum C_T/σ, 120 kn.

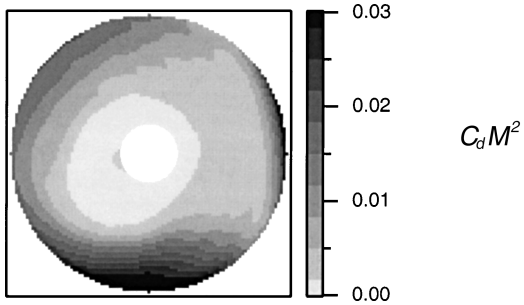

a) 22,000 lb; $\Omega = 25.6$ rad/s; $A_2 = 2.34$ deg; and $\phi_2 = 56.65$ deg

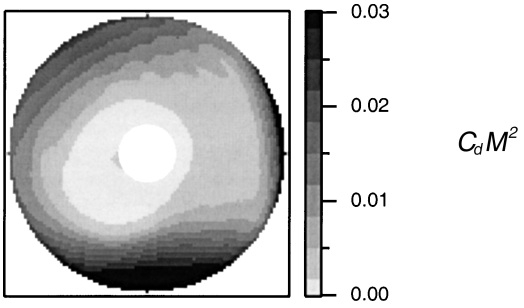

b) 24,500 lb; $\Omega = 27$ rad/s; $A_2 = 2.42$ deg; and $\phi_2 = 55.48$ deg

Fig. 8 Local drag distribution at maximum C_T/σ, 120 kn.

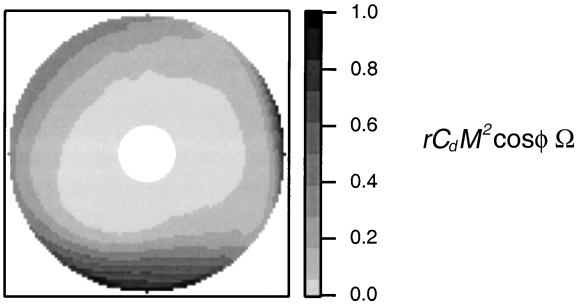

a) 22,000 lb; $\Omega = 25.6$ rad/s; $A_2 = 2.34$ deg; and $\phi_2 = 56.65$ deg

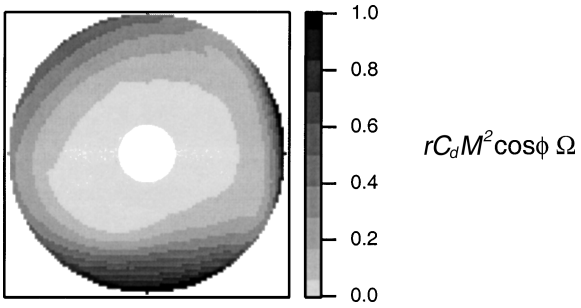

b) 24,500 lb; $\Omega = 27$ rad/s; $A_2 = 2.42$ deg; and $\phi_2 = 55.48$ deg

Fig. 9 Local contributions to profile power, at maximum C_T/σ, 120 kn.

Effects of Refined Rotor Modeling

Effects of Refined Inflow Modeling

All of the results presented thus far were obtained with a three-state linear inflow model. To investigate the effect of nonlinear inflow, parametric studies were performed with two-per-revolution inputs for both the 16,000- and 22,000-lb cases at an advance ratio $\mu = 0.28$ with a refined wake model. The two-per-revolution amplitude was fixed at 1 deg, and the two-per-revolution phase angle was changed from 0 deg to 360 deg in 30-deg increments. The nonlinear inflow used in this study is the Bagai–Leishman–Park free wake model.[18] Figures 10 and 11 show the results of the parametric study for the 16,000- and 22,000-lb cases. The solid circles are the results obtained with the linear inflow model, and the open circles are

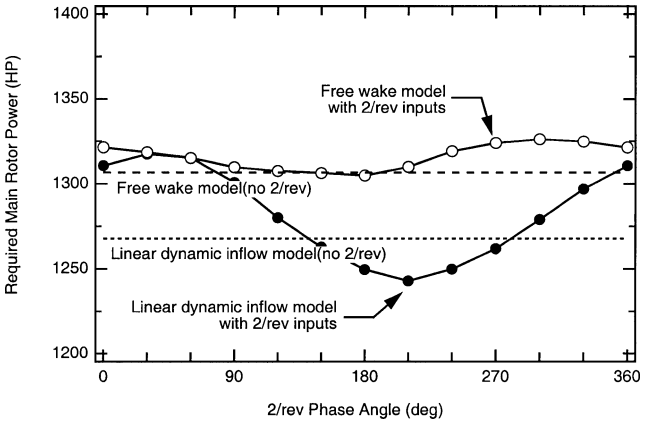

Fig. 10 Effect of nonlinear inflow on prediction of required rotor power: 16,000 lb; 120 kn; and $A_2 = 1$ deg.

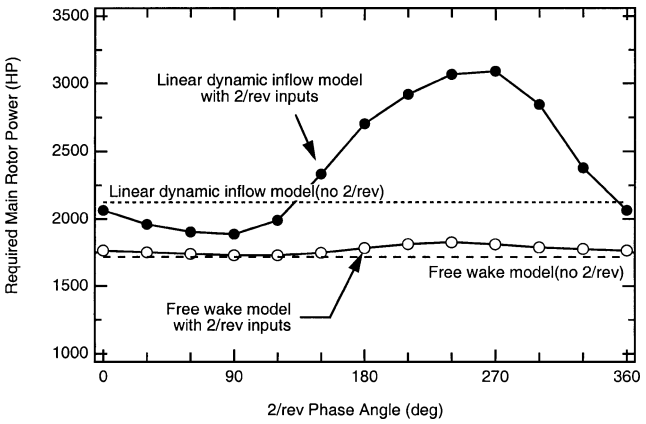

Fig. 11 Effect of nonlinear inflow on prediction of required rotor power: 22,000 lb; 120 kn; and $A_2 = 1$ deg.

those obtained from the free wake model. Figures 10 and 11 show that, although there are noticeable differences in the required power predictions, the optimum phases of the two-per-revolution input for minimum power predicted in the two cases appear to be quite close, that is, within 30 deg. This holds true for both the 16,000- and the 22,000-lb cases. Because the computational effort is obviously much higher with a free wake model, the most efficient strategy for the optimization of the two-per-revolution input for minimum power may be to perform an initial parametric study (or to carry out the initial phases of the optimization) by the use of a simplified, linear inflow model and then to refine the two-per-revolution calculations and to compute the actual required power with the more sophisticated free wake model. Because the predictions with the free wake model are likely to be more accurate than those based on linear inflow, Figs. 10 and 11 also indicate that the actual benefits achieved with the two-per-revolution input may be smaller than predicted by the use of linear inflow.

To further investigate the differences in the predictions obtained with the two aerodynamic models, rotor maps of $\Delta r C_D M^2 \cos\phi$ and $\Delta r C_l M^2 \sin\phi$ are plotted in Figs. 12 and 13 for the 16,000-lb case at $\phi_2 = 210$ deg and in Figs. 14 and 15 for the 22,000-lb case at $\phi_2 = 90$ deg. The symbol Δ in Figs. 12–15 denotes the difference between the value of a quantity when the two-per-revolution input is applied and the baseline value. Recall that $rC_D M^2 \cos\phi$ and $rC_l M^2 \sin\phi$ are proportional to the local contribution to the profile rotor torque, and to the induced rotor torque, respectively. Multiplied by the rotor speed, assumed to be constant in this study, and integrated over the rotor disk, these quantities give the total profile and induced power.

Figure 12a is the perturbation of local profile torque with the free wake model and Fig. 12a, the linear inflow model. There is very little difference over most of the disk when the rotor maps of

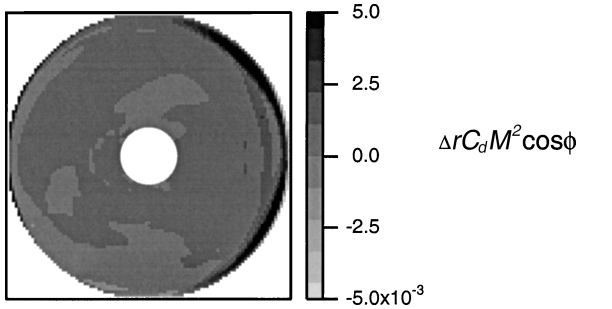

a) Free wake inflow model, baseline case

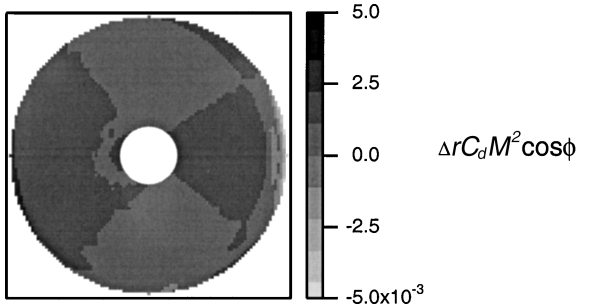

b) Linear inflow model, baseline case

Fig. 12 Perturbation of profile torque distribution: 16,000 lb; 120 kn; $A_2 = 1$ deg; and $\phi_2 = 210$ deg.

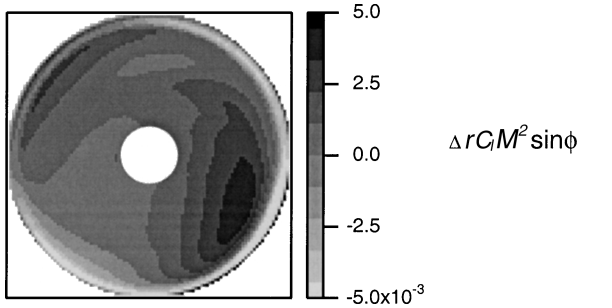

a) Free wake inflow model, baseline case

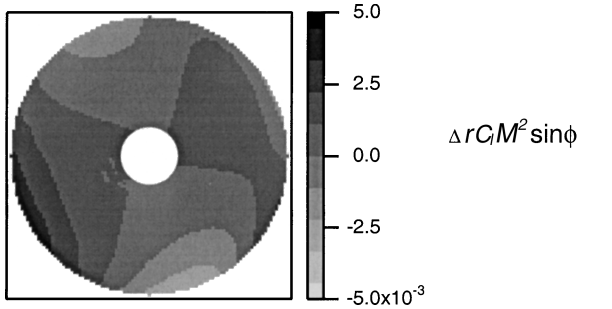

b) Linear inflow model, baseline case

Fig. 13 Perturbation of induced torque distribution: 16,000 lb; 120 kn; $A_2 = 1$ deg; and $\phi_2 = 210$ deg.

$\Delta r C_D M^2 \cos\phi$ are compared, except for the large increments in the blade tip region on the advancing side of the disk. In terms of total profile power, the difference is very small when compared to the $\Delta r C_l M^2 \sin\phi$ shown in Fig. 13. Figure 13b illustrates the perturbation of induced torque with the linear inflow model. Figure 13b shows that the induced torque largely remains unchanged over most of the disk. There are slight reductions of induced torque at the front and rear sides of the disk and a large increment at the retreating side of the disk. In contrast, the perturbation from the free wake model (Fig. 13a) shows significant increases at the outboard portion of blade at the advancing and retreating sides of the disk. In terms of total value (as opposed to perturbations when the two-per-revolution

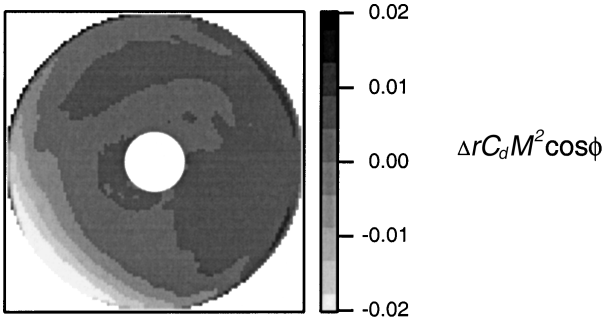

a) Free wake inflow model, baseline case

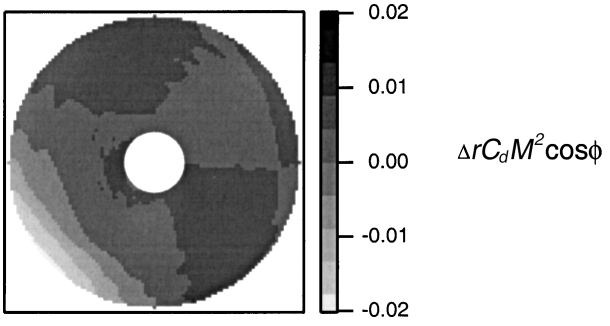

b) Linear inflow model, baseline case

Fig. 14 Perturbation of profile torque distribution: 22,000 lb; 120 kn; $A_2 = 1$ deg; and $\phi_2 = 90$ deg.

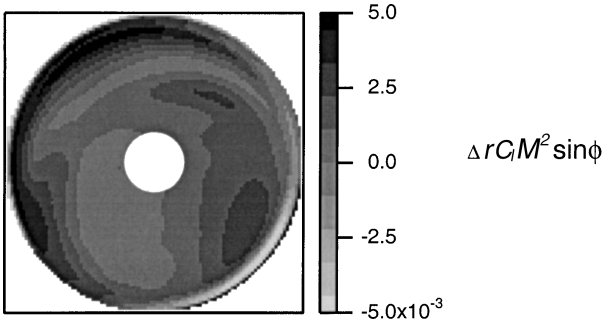

a) Free wake inflow model, baseline case

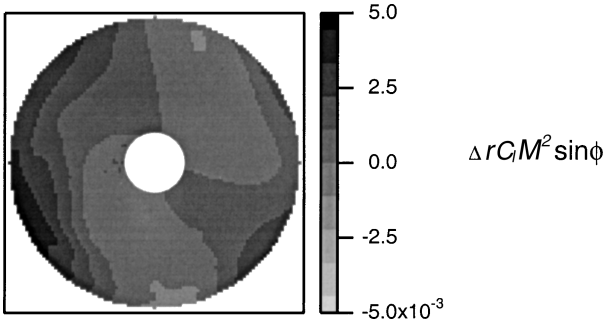

b) Linear inflow model, baseline case

Fig. 15 Perturbation of induced torque distribution: 22,000 lb; 120 kn; $A_2 = 1$ deg; and $\phi_2 = 90$ deg.

input is applied) the induced power calculated from the free wake model is six times larger than that from linear inflow model. The difference in total required power for $\phi_2 = 210$ deg in Fig. 10 comes mainly from the difference of the prediction in induced power.

The difference in total power required for the 22,000-lb case at the optimum two-per-revolution phase angle are similar to the 16,000-lb case. The source of this difference can also be determined by the same procedure as that applied to the 16,000-lb case. Figure 14 shows the perturbation of the $rC_D M^2 \cos\phi$ distribution. The profile power decreases primarily because of a reduction in the contributions of the outboard regions in the fourth quadrant; magnitude and disk location of this reduction are predicted in a very similar way with both aerodynamic models. The perturbation from the free wake model (Fig. 14a) shows a small increase over a larger area, which occurs at the tip over most of the first and fourth quadrant. Overall, the total profile power calculated from the free wake model is lower than that of the linear inflow model.

The perturbation of the induced power is shown in Fig. 15. Figure 15a shows that the free wake model predicts a higher value of induced torque over the entire disk, except at the tip region around $\psi = 45$ deg. On the other hand, the perturbation from the linear inflow model (Fig. 15b) remains unchanged over most of the rotor disk. Most of the increase occurs at the retreating side of the disk. The two-per-revolution input produces perturbations in profile power that are much larger than those in induced power. In terms of total induced power, the calculation from the free wake model predicts twice as much induced power as the linear inflow model. However, this increment is not much larger than the underprediction from the profile power calculation. Therefore, there is no single dominant term that contributes to the difference shown in Fig. 11 at $\phi_2 = 90$ deg. The difference in power required for the 22,000-lb case is the combined effect of the changes in profile and induced power.

Effects of Blade Flexibility

All of the results presented thus far were obtained with a rigid flap–lag blade model. To investigate the effect of blade flexibility on the results, parametric studies were performed with two-per-revolution inputs for both the 16,000- and 22,000-lb cases at $\mu = 0.28$. The two-per-revolution amplitude was fixed at 1 deg, and the two-per-revolution phase angle was changed from 0 to 360 deg in 30-deg increments. A coupled flap–lag–torsion flexible blade model was included; two rigid-body modes and the three lowest frequency elastic modes were used, for a total of five blade modes. The control system was assumed to be infinitely rigid, and the effect of the lag damper was neglected. Table 3 lists the modes that are included in the current analysis, including natural frequency and type for each mode.

Figures 16 and 17 show the results of the parametric study for the 16,000- and 22,000-lb cases. The solid circles are the results

Table 3 UH-60A blade natural frequencies

Mode	Frequency per revolution	Mode type
1	0.2677	Rigid lag
2	1.0351	Rigid flap
3	2.8189	First flap
4	4.6591	First lag
5	5.1821	First torsion

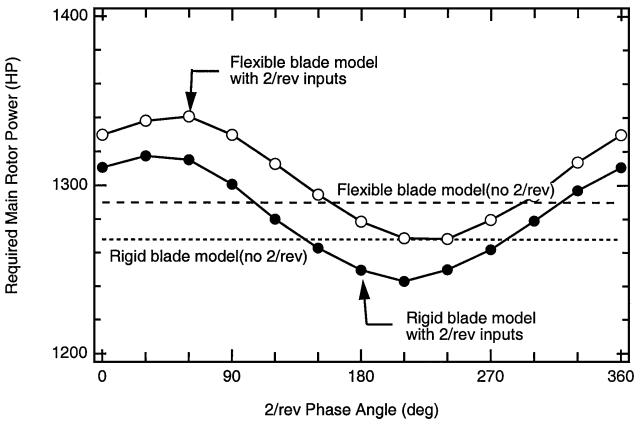

Fig. 16 Effect of blade flexibility on prediction of rotor power: 16,000 lb; 120 kn; and $A_2 = 1$ deg.

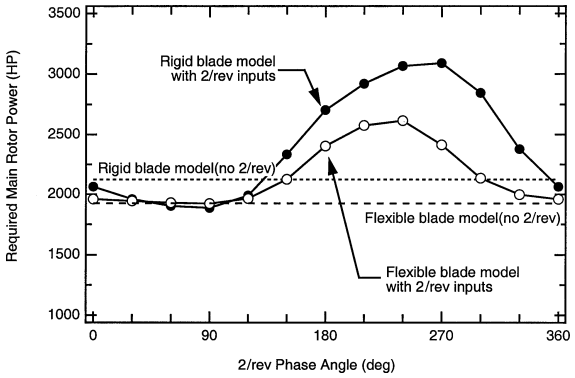

Fig. 17 Effect of blade flexibility on prediction of rotor power: 22,000 lb; 120 kn; and $A_2 = 1$ deg.

obtained using the rigid blade model, and the open circles are those obtained using the flexible blade model. Figures 16 and 17 show that the optimum phases of the two-per-revolution input for minimum power predicted in the two cases appear to be quite close, that is, within 30 deg. This holds true for both the 16,000- and the 22,000-lb cases. As in the case of the inflow modeling, the most efficient strategy for the optimization of the two-per-revolution input for minimum power seems to be performing an initial parametric study (or carrying out the initial phases of the optimization) using the less computationally demanding rigid blade model, and then refining the two-per-revolution calculations and computing the actual required power using the more sophisticated flexible blade model (Figs. 18–21). Because no other helicopter configurations were explored, these conclusions are limited to the Sikorsky UH-60; all of the other simplifying modeling assumptions mentioned earlier should also be taken into account.

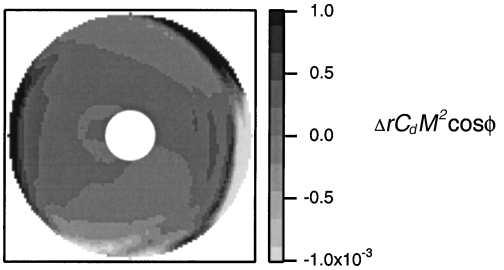

a) Flexible blade model, baseline case

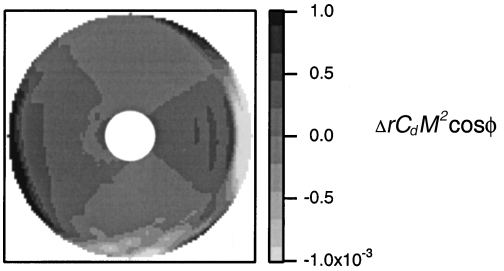

b) Rigid blade model, baseline case

Fig. 18 Local contributions to profile power: 16,000 lb; 120 kn; $A_2 = 1$ deg; and $\phi_2 = 210$ deg.

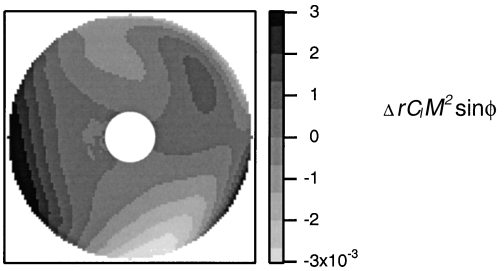

a) Flexible blade model, baseline case

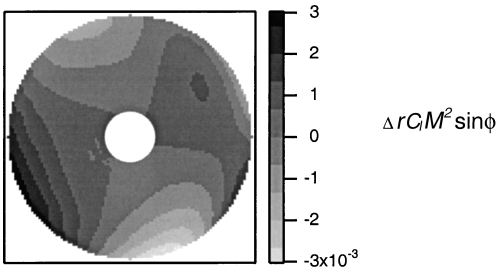

b) Rigid blade model, baseline case

Fig. 19 Local contributions to induced power: 16,000 lb; 120 kn; $A_2 = 1$ deg; and $\phi_2 = 210$ deg.

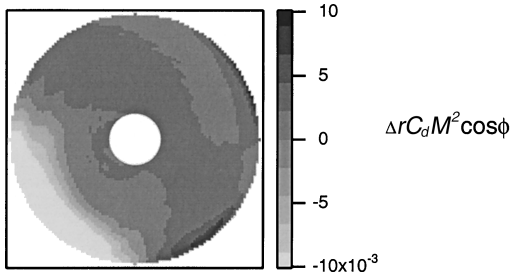

a) Flexible blade model, baseline case

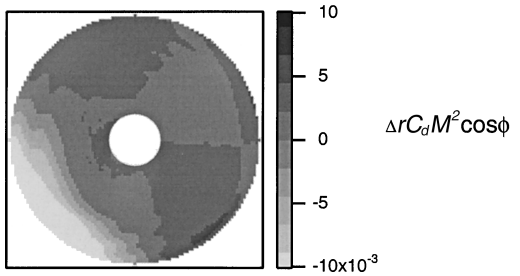

b) Rigid blade model, baseline case

Fig. 20 Local contributions to profile power: 22,000 lb; 120 kn; $A_2 = 1$ deg; and $\phi_2 = 90$ deg.

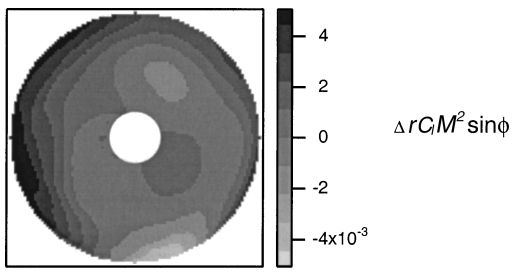

a) Flexible blade model, baseline case

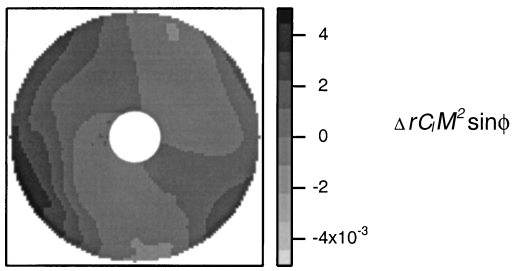

b) Rigid blade model, baseline case

Fig. 21 Local contributions to induced power: 22,000 lb; 120 kn; $A_2 = 1$ deg; and $\phi_2 = 90$ deg.

Conclusions

This paper presented the results of a study to determine the optimum two-per-revolution input required to minimize rotor power, maximize thrust, or minimize rotor speed. Formal numerical optimization techniques were used for this purpose. The impact of improved rotor modeling on the prediction of the effects of two-per-revolution input on rotor power was also addressed, in particular, the effect of using a free wake inflow model, and a flexible rotor blade model.

The main conclusions of the present study are as follows:

1) The optimization for optimum two-per-revolution input is best carried out by calculation of the trim problem for every value of the input proposed by the optimizer, as opposed to including the trim calculations as equality constraints in the optimization. The latter leads to optimization procedures with poor numerical properties.

2) An appropriate two-per-revolution input can increase the rotor maximum thrust. With the optimum two-per-revolution input, the simulation model with simplified aerodynamics predicts that the helicopter can be trimmed at high speed at a weight that is about 11% greater than the maximum trimmable weight without the two-per-revolution input. The primary physical mechanism through which the two-per-revolution input affects thrust is the change in lift distribution over the rotor disk; the additional thrust is generated at the front and the rear of the rotor disk. However, simulations with a more sophisticated, free wake-based aerodynamic model indicate smaller benefits.

3) If the two-per-revolution input is used to reduce rotor speed, an appropriate two-per-revolution input can also further reduce the rotor speed compared with a case without such an input. The physical mechanism is the same as in the optimization for maximum thrust, and the maximum value of C_T/σ is also the same. Therefore, a two-per-revolution input helps increase the maximum C_T/σ capabilities of the helicopter, and this can be exploited to increase thrust, reduce rotor speed, or both.

4) Although the power predictions obtained with a free wake model are different from those obtained with a simpler linear inflow model, the accuracy of the optimum two-per-revolution input predicted by the use of the simpler model is adequate. At least for the configuration and the type of problems shown in this paper, the best practical strategy to optimize the two-per-revolution input is to conduct an initial study with a simple linear inflow model and then refine it with the more sophisticated one. The same conclusions appear to hold for more sophisticated flexible blade models, just as they do with simpler rigid blade ones.

Acknowledgments

This research was supported by the U. S. Army Aeroflightdynamics Directorate, NASA Ames Research Center, Moffett Field, California, under Grant NAG 2-1231. The authors would like to thank the Grant Monitor, Mark Tischler, for many useful comments and discussions.

References

[1]Friedmann, P. P., and Millot, T. A., "Vibration Reduction in Rotorcraft Using Active Control: A Comparison of Various Approaches," *Journal of Guidance, Control, and Dynamics*, Vol. 18, No. 4, 1995, pp. 664–673.

[2]Teves, D., Niesl, G., Blaas, A., and Jacklin, S., "The Role of Active Control in Future Rotorcraft," *Proceedings of the Twenty-first European Rotorcraft Forum*, St. Petersburg, Russia, 1995, pp. III, 10.1–17.

[3]Stewart, W., "Second Harmonic Control in the Helicopter Rotor," Aeronautical Research Council R&M 2997, London, England, U.K., 1952.

[4]Payne, P. R., "Higher Harmonic Rotor Control," *Aircraft Engineering*, Vol. 30, Aug. 1958, p. 354.

[5]Arcidiacono, P. J., "Theoretical Performance of Helicopters Having Second and Higher Harmonic Feathering Control," *Journal of the American Helicopter Society*, Vol. 6, No. 2, 1961, pp. 8–19.

[6]Ham, N. D., "Helicopter Individual Blade Control Research at MIT: 1977–1985," *Vertica*, Vol. 11, Nos. 1 and 2, 1987, pp. 109–122.

[7]Ham, N. D., "Helicopter Stall Alleviation Using Individual Blade Control," *Proceedings of the Tenth European Rotorcraft Forum*, 1984.

[8]Shaw, J., Albion, N., Hanker, E. J., Jr., and Teal, R. S.,"Higher Harmonic Control: Wind Tunnel Demonstration of Fully Effective Vibratory Hub Force Suppression," *Proceedings of the American Helicopter Society 41st Annual Forum*, American Helicopter Society, Alexandria, VA, 1985, pp. 1–16.

[9]Nguyen, K. Q., and Chopra, I., "Effects of Higher Harmonic Control on Rotor Performance and Control Loads," *Journal of Aircraft*, Vol. 29, No. 3, 1992, pp. 336–342.

[10]Polychroniadis, M., "Generalized Higher Harmonic Control—Ten Years of Aerospatiale Experience," *Proceedings of the Sixteenth European Rotorcraft Forum*, 1990.

[11]Jacklin, S. A., Nguyen, K. Q., Blass, A., and Richter, P., "Full-Scale Wind Tunnel Test of a Helicopter Individual Blade Control System," *Proceedings of the American Helicopter Society 50th Annual Forum*, American Helicopter Society, Alexandria, VA, 1994, pp. 579–596.

[12]Jacklin, S. A., Blass, A., Swanson, S. M., and Teves, D., "Second Test of a Helicopter Individual Blade Control System in the NASA Ames 40- by 80-foot Wind Tunnel," *Proceedings of the American Helicopter Society 2nd International Aeromechanics Specialists' Conference*, American Helicopter Society, Alexandria, VA, 1995, pp. 7-9–7-26.

[13]Cheng, R. P., Theodore, C. R., and Celi, R., "Effects of Higher Harmonic Control on Rotor Performance," *Proceedings of the 56th Annual Forum of the American Helicopter Society*, American Helicopter Society, Alexandria, VA, 2000.

[14]Kim, F. D., Celi, R., and Tischler, M. B., "High Order State Space Simulation Models of Helicopter Flight Mechanics," *Journal of the American Helicopter Society*, Vol. 38, No. 2, 1993, pp. 16–27.

[15]Kim, F. D., Celi, R., and Tischler, M. B., "Forward Flight Trim Calculation and Frequency Response Validation of a High-Order Helicopter Simulation Model," *Journal of Aircraft*, Vol. 30, No. 6, 1993, pp. 854–863.

[16]Vanderplaats, G. N., *Numerical Optimization Techniques for Engineering Design: With Applications*, McGraw–Hill, New York, 1984, Chap. 6.

[17]Vanderplaats, G. N., *DOT—Design Optimization Tools, User's Manual*, VMA Engineering, Inc., Goleta, CA, 1995.

[18]Bagai, A., Leishman, J. G., and Park, J., "Aerodynamic Analysis of a Helicopter in Steady Maneuvering Flight Using a Free-Vortex Rotor Wake Model," *Journal of the American Helicopter Society*, Vol. 44, No. 2, 1999.